Carcinogenesis, 2015, Vol. 36, No. 10, 1223–1234

doi:10.1093/carcin/bgv113
Advance Access publication August 4, 2015
Original Manuscript

ORIGINAL MANUSCRIPT

Aschantin targeting on the kinase domain of mammalian target of rapamycin suppresses epidermal growth factor-induced neoplastic cell transformation

Cheol-Jung Lee[1,†], Jeong-Hoon Jang[1,2,†], Ji-Young Lee[1], Mee-Hyun Lee[1], Yan Li[3], Hyung Won Ryu[4], Kyung-Il Choi[1], Zigang Dong[3], Hye Suk Lee[1], Sei-Ryang Oh[4], Young-Joon Surh[2] and Yong-Yeon Cho[1,*]

[1]College of Pharmacy, The Catholic University of Korea, 43, Jibong-ro, Wonmi-gu, Bucheon-si, Gyeonggi-do 420-743, Republic of Korea, [2]College of Pharmacy, Seoul National University, 1, Gwanak-ro, Gwanak-gu, Seoul 151-742, Republic of Korea, [3]The Hormel Institute, University of Minnesota, 801, 16th AVE, NE, Austin, MN 55912, USA and [4]Natural Medicine Research Center, Korea Research Institute of Bioscience & Biotechnology, 30 Yeongudanji-ro, Ochang-eup, Cheongwon-gun, ChungBuk 363-883, Republic of Korea

[*]To whom correspondence should be addressed. Tel: +82 2 2164 4092; Fax: +82 2 2164 4059; Email: yongyeon@catholic.ac.kr

[†]These authors contributed equally to this work.

Correspondence may also be addressed to Young-Joon Surh. Tel:+82 2 880 7845; Fax: +82 2 874 9775; Email: surh@plaza.snu.ac.kr

Abstract

Mammalian target of rapamycin (mTOR), a serine/threonine protein kinase, forms two different complexes, complex 1 and 2, and plays a key role in the regulation of Akt signaling-mediated cell proliferation and transformation. This study reveals aschantin, a natural compound abundantly found in *Magnolia* flos, as a novel mTOR kinase inhibitor. Aschantin directly targeted the active pocket of mTOR kinase domain by competing with adenosine triphosphate (ATP), but not PI3K and PDK1. Aschantin inhibited epidermal growth factor (EGF)-induced full activation of Akt by phosphorylation at Ser473/Thr308, resulting in inhibition of the mTORC2/Akt and Akt/mTORC1/p70S6K signaling pathways and activation of GSK3β by abrogation of Akt-mediated GSK3β phosphorylation at Ser9. The activated GSK3β inhibited cell proliferation by c-Jun phosphorylation at Ser243, which facilitated destabilization and degradation of c-Jun through the ubiquitination-mediated proteasomal degradation pathway. Notably, aschantin treatment decreased c-Jun stability through inhibition of the mTORC2-Akt signaling pathway, which suppressed EGF-induced anchorage-independent cell transformation in non-malignant JB6 Cl41 and HaCaT cells and colony growth of LNCaP and MIAPaCa-2 cancer cells in soft agar. Altogether, the results show that aschantin targets mTOR kinase and destabilizes c-Jun, which implicate aschantin as a potential chemopreventive or therapeutic agent.

Introduction

Mammalian target of rapamycin (mTOR) is a serine/threonine protein kinase with two different complexes, mTORC1 and mTORC2. mTORC1 is a molecular target of allosteric inhibitor rapamycin (1). mTORC2 is a direct kinase of Akt Ser473 phosphorylation, resulting in full activation of Akt (1). mTOR plays essential roles in cell proliferation, cell transformation, protein synthesis and nutritional level sensory response (2). Activating mutations of receptor tyrosine kinases (RTKs) and phosphoinositol-3-kinase (PI3K) and inactivating mutation of phosphatase and tensin homolog (PTEN) cause cancer development in many

Received: April 29, 2015; **Revised:** July 17, 2015; **Accepted:** July 27, 2015

Abbreviations

AP-1	activator protein-1
ATP	adenosine triphosphate
BME	Basal Medium Eagle
EGF	epidermal growth factor
ERK	extracellular signal-regulated kinase
FBS	fetal bovine serum
JNK	c-Jun N-terminal kinase
MEF	mouse embryonic fibroblast
mTOR	mammalian target of rapamycin

different organs by upregulating the Akt/mTOR signaling pathway (3). Inhibition of mTORC1 by rapamycin and its analogues induces hyperactivation of Akt, indicative of a negative feedback loop between p70S6K1 and IRS1 in DU-145 prostate cancer cells (4), suggesting that antitumor activities of therapeutic compounds targeting the Akt signaling pathway might be required for inhibition of Akt/mTORC1 and mTORC2/Akt signaling pathways.

Several selective adenosine triphosphate (ATP)-competitive inhibitors have been developed to target the kinase domain of mTORC1 and mTORC2 (5). Torin1 blocks mTORC1 and mTORC2 with an IC_{50} of about 2 and 10 nM, respectively, resulting in inhibition of the Akt phosphorylation at Ser473 (6). PP242 produces a better therapeutic response than rapamycin with a milder effect on normal lymphocytes (7). Since mTOR allosteric inhibitors suppressing mTORC1 activity suppress the p70S6K-mediated feedback loop, mTORC1 inhibition enhances 3-phosphoinositide dependent protein kinase-1 (PDK1)-mediated phosphorylation of AKT at Thr308 (8). Thus, mTORC2 specific inhibitor might block the pro-survival functions of mTORC2 without inhibiting mTORC1, resulting in no disruption of the p70S6K-IRS1 feedback loop and no hyperactivation of PI3K (8).

Currently, dual PI3K-mTOR catalytic inhibitors may be an ideal therapeutic compound because PI-103 and NVP-BEZ235 suppress both p70S6K and AKT activation (9,10), resulting in inhibition of cancer cell proliferation more efficiently than rapamycin or LY294002, a PI3K inhibitor (8). However, this broad inhibition may be toxic to normal cells. Therefore, non-toxic mTORC catalytic inhibitors may improve the cancer therapy against broad range of human cancers.

c-Jun, a central component of the mammalian transcription factor activator protein-1 (AP-1) complex, plays a key role in the regulation of cell proliferation, transformation and cancer development (11). Environmental stresses including ultraviolet light, growth factors and cytokines activate mitogen-activated protein kinase (MAPK) signaling pathways (12). The activated extracellular signal-regulated kinases (ERKs) transduce their activation signal to downstream target transcription factors, including ATF-1, c-Fos and c-Jun, through p90RSKs, such as p90RSK2 (13). Since the AP-1 complex regulates about 60% of the tumorigenesis-related gene expression in eukaryotic cells, the signaling pathways to regulate AP-1 transactivation activity are of special interest in cancer therapy. Non-small-cell lung cancer and human bronchial epithelial cancer cell lines frequently overexpressed c-Jun, and forced expression of c-Jun increases cell proliferation and colony formation in soft agar (14). Our previous study demonstrated that increased AP-1 transactivation activity induces the anchorage-independent cell transformation in JB6 Cl41 mouse skin epidermal cells (15). Importantly, phosphorylation of c-Jun C-terminus at Ser243 by GSK3β leads to Fbxw7 binding and degradation of c-Jun (16). Thus, signaling pathways regulating c-Jun/AP-1 transactivation activity and protein stability have been considered to be an important target as chemopreventive and therapeutic agents of cancer.

Aschantin (CID122643; 5-[(1s,3ar,4s,6ar)-4-(3,4,5-trimethoxyphenyl)tetrahydro-1h,3h-furo[3,4-c]furan-1-yl]-1,3-benzodioxole) is a natural compound abundantly found in *Magnolia* flos (Korean name: Shin-Yi), a commonly used traditional Chinese medicine to cure nasal congestion with headache, sinusitis and allergic rhinitis (17). Recently, we demonstrated that magnolin (CID169234; (1s,3ar,4s,6ar)-1-(3,4-dimethoxyphenyl)-4-(3,4,5-trimethoxyphenyl)tetrahydro-1h,3h-furo[3,4-c]furan) targets active pockets of ERK1 and ERK2, and inhibits kinase activities of ERK1 and ERK2 with a IC_{50} of 87 and 16.5 nM, respectively (18). Although aschantin has an apparently similar structure to magnolin, the physiological role of aschantin has not been clearly defined, particularly in carcinogenesis.

In this study, aschantin targeted the kinase active pocket of mTOR, resulting in inhibition of mTORC2/Akt and Akt/mTORC1/p70S6K signaling pathways without cytotoxicity. Inhibition of mTORC2-mediated Akt activity enhanced c-Jun degradation through GSK3β mediated c-Jun phosphorylation at Ser243 and ubiquitination-dependent proteasomal degradation pathway.

Materials and methods

Aschantin

Aschantin was extracted from dried flower buds of *Magnolia fargesii* as described previously (19). Purity >99.0% was confirmed by high-performance liquid chromatography (HPLC) by Dr S.-R. Oh, Korea Research Institute of Bioscience and Biotechnology. The highly purified aschantin was prepared at a concentration of 100 mM (stock solution) by dissolution in dimethylsulfoxide (Sigma–Aldrich, St Louis, MO) and stored at −20°C. Before utilization, aschantin was freshly diluted with media to the appropriate concentrations and was used to treat cells. The final concentration of dimethylsulfoxide comprised over 0.1% of the total medium volume.

Cell culture and transfection

JB6 Cl41 mouse skin epidermal cells, HaCaT human skin keratinocytes, human pancreatic cancer cells (MIAPaCa-2, AsPC-1 and BxPC-3) and human prostate cancer cells (DU-145 and LNCaP) were obtained from the American Type Culture Collection (Manassas, VA). $GSK3\beta^{+/+}$ and $GSK3\beta^{-/-}$ mouse embryonic fibroblasts (MEFs) were generously provided by Dr Eui-Ju Choi (Korea University, Seoul, Korea) through the MTA with Dr J.W. Woodgett, Mount Sinai Hospital & the Samuel Lunenfeld Research Institute. JB6 Cl41 cells were cultured in 5% fetal bovine serum (FBS)-minimum essential medium (MEM). HaCaT, and $GSK3\beta^{+/+}$ and $GSK3\beta^{-/-}$ MEFs were cultured with 10% FBS-Dulbecco's modified Eagle's medium (DMEM) and antibiotic at 37°C in a 5% CO_2 incubator. MIAPaCa-2 cells were cultured in 10% FBS and 2.5% horse serum-DMEM and LNCaP-FGC, AsPC-1, BxPC-3 cells were cultured with 10% FBS-RPMI 1640. DU-145 cells were cultured in 10% FBS-MEM. The cells were maintained by splitting at 90% confluence and changing the media every other day. These cell lines were used at passage <15 and were periodically authenticated by monitoring of cell morphology, growth curve analysis and contamination inspection such as mycoplasma. When cells were reached 60% confluence, the expression vectors were transfected using jetPEI (Polyplus-Transfection, New York, NY) according to the manufacturer's instructions.

Anchorage-independent cell transformation assay

Epidermal growth factor (EGF)-induced cell transformation was performed in JB6 Cl41 and HaCaT cells. Briefly, cells (8×10^3/ml) were exposed to EGF (10 ng/ml) and/or indicated doses of aschantin in 1 ml of 0.3% Basal Medium Eagle (BME) agar containing 10% FBS. MIA PaCa-2 cells and LNCaP-FGC cells (8×10^3/well) were suspended in 10% FBS and 2.5% horse serum-DMEM and 10% FBS-RPMI 1640 media were added to 0.3% agar with or without indicated doses of aschantin. The cultures were maintained at 37°C in a 5% CO_2 incubator for 10–14 days, and the cell colonies were scored using an ECLIPSE Ti inverted microscope and the NIS-Elements AR

(V. 4.0) computer software program (NIKON Instruments Korea, Gangnam, Seoul, Korea) as described previously (20).

Computational docking of aschantin

The crystal structures of two proteins were obtained from Protein Data Bank, PDB entries: 4JT6 (mTOR) 3HHM (PI3K) and 1JM6 (PDK1). The crystal structures were prepared using the Protein Preparation Wizard in Maestro v9.4. Hydrogen atoms were added consistent with a pH of 7. All water molecules were removed. Then the structure was minimized with a root mean square deviation cutoff value of 0.3 Å. The Glide v5.9 program was used for ligand docking. The receptor grid was created with the centroid of the crystal ligand as the center of the grid. Flexible docking was performed in the extra precision mode. Number of poses per ligand was set to 10 in post-docking minimization and at most one pose as the output. The other parameters were kept as defaults.

In vitro kinase assay

Active mTOR (50 ng) or active PDK1 (50 ng) was combined with Akt (400 ng) purified from *Escherichia coli* as a substrate, 100 μM of cold ATP and the indicated doses of aschantin in a 20 μl reaction mixture. The kinase reaction was conducted at 30°C for 30 min and stopped by adding 6× sodium dodecyl sulfate (SDS)-sample buffer and boiling. The proteins were resolved by 8–10% SDS-polyacrylamide gel electrophoresis (SDS-PAGE) and visualized by western blotting using specific antibody against phospho-Ser473 or -Thr308 as indicated. The band intensities were measured by the NIH Image J ver. 1.37 computer program, and the IC_{50} level of aschantin on the mTOR kinase activities was calculated based on the band intensities. The PI3K inhibitor assay was conducted according to the manufacturers' suggested protocol (EMD Millipore, Billerica, MA). Briefly, PI3K and indicated doses of aschantin were combined into each well and preincubated for 10 min. The premixtures were combined with PIP2 substrate and incubated for 1 h at room temperature. After incubation, GRP1 was added either in the presence or absence of biotinylated-PIP3/EDTA as indicated, and kinase reaction was conducted at room temperature for 1 h. The kinase activities in indicated doses of aschantin were measured at OD_{450} nm using a TMB substrate.

ATP-agarose bead binding assay

The ATP-agarose binding assay was conducted in 500 μl of incubation buffer [10 mM Tris–HCl (pH 7.5), 50 mM KCl, 5 mM $MgCl_2$, 2 mM dithiothreitol and 0.01% NP-40]. Active mTOR kinase (100 ng) and indicated doses of aschantin were preincubated overnight at 4°C and incubated for 2.5 h at 25°C, which was followed by the addition of ATP-agarose beads or control-beads (50% slurry) (Innova Biosciences, Cambridge, UK). The beads were washed three times for 5 min at 4°C with incubating buffer and the proteins were denatured by adding 6× SDS buffer and boiling for 5 min. The mTOR kinase was visualized by western blotting using the indicated specific antibodies.

Quantitative real-time PCR

JB6 Cl41 and LNCaP cells (1×10^5) were seeded into 60-mm dishes, cultured overnight and starved for 16 h with 0.1% FBS. The cells pretreated with indicated doses of aschantin for 30 min were stimulated with EGF (10 ng/ml) or EGF (10 ng/ml) and indicated doses of aschantin. Cycloheximide (CHX, 10 μg/ml), a protein synthesis inhibitor, and MG132, a proteasome inhibitor, were cotreated together with EGF for 30 min. The cells were harvested and total RNAs were extracted using Trizol Reagent (Invitrogen, Carlsbad, CA). c-Jun gene expression was analyzed with 50 ng of total RNA and a c-Jun specific real-time primer set (Mm00495062_s1; Applied Biosystems, Foster City, CA) or a glyceraldehyde 3-phosphate dehydrogenase (GAPDH)-specific real-time primer set (Mm99999915_g1; Applied Biosystems) by quantitative one-step real-time PCR using the TaqMan RNA-to-C_T 1-step kit (Applied Biosystems) following the manufacturer's suggested protocols. The C_T values of *c-jun* gene expression were normalized with the C_T values of *gapdh*, an internal control to monitor equal RNA utilization.

Immunoprecipitation

JB6 Cl41 cells were seeded into 100-mm dishes and cultured overnight. The cells were transfected with *pHA*-ubiquitin expression plasmids using jetPEI, and cultured for 24 h. The cells were cotreated with indicated doses of aschantin and MG132 (10 μM) for 6 h. The cells were disrupted with NP-40 lysis buffer (150 mM NaCl, 40 mM Tris–HCl pH 8.0 and 0.5% NP-40), and then immunoprecipitation was conducted with the equal amount of proteins and indicated specific antibodies. The precipitated proteins were resolved by 10% SDS-PAGE and visualized by western blotting using the indicated specific antibodies.

KinaseProfiler™ assay against aschantin

To confirm the specificity of aschantin, KinaseProfiler™ Service (EMD Millipore) was used with different available kinases (http://www.millipore.com/drugdiscovery/dd3/KinaseProfiler) including JNK1α1, JNK2α2, MAPK1, MAPK2, PKBα, PKBβ and SAPK2α. The screening was performed with 10 μM of aschantin and kinase substrates according to the manufacturer's protocol.

Results

Aschantin suppresses cell proliferation by inhibition of G_1/S cell cycle transition in JB6 Cl41 cells

Although aschantin, a natural compound abundantly found in Shin-Yi (21), has a similar chemical structure with magnolin (Figure 1A), the biological activity of aschantin in cancer is unknown. Aschantin suppressed proliferation of JB6 Cl41 cells in a dose-dependent manner (Figure 1B). Flow cytometry analysis revealed that aschantin induced the accumulation of G_1/G_0 cell cycle phase and suppressed the S cell cycle phase in the cell population compared to that of the vehicle dimethylsulfoxide-treated control cells (Figure 1C and Supplementary Figure 1A, available at *Carcinogenesis* Online). Synchronization by starvation and cell cycle release by EGF demonstrated that EGF stimulation increased S cell cycle phase from 30 to 50% and suppressed G_1/G_0 cell cycle phase from 65 to 53% compared to vehicle treated control cells (Figure 1D and Supplementary Figure 1B, available at *Carcinogenesis* Online). Notably, the increased S phase cell cycle by EGF stimulation was inhibited by cotreatment with EGF and aschantin in a dose-dependent manner. Aschantin concentrations >15 μM totally abrogated the EGF stimulatory effect of S phase accumulation (Figure 1D and Supplementary Figure 1B, available at *Carcinogenesis* Online). Additionally, aschantin induced a marginal increase of G_2/M phase population (Figure 1D and Supplementary Figure 1, available at *Carcinogenesis* Online); the vehicle had no effect on the cell cycle distribution (Figure 1C andD and Supplementary Figure 1, available at *Carcinogenesis* Online), and aschantin had no cytotoxic effects in JB6 Cl41 cells (Supplementary Figure 2, available at *Carcinogenesis* Online). These results indicated that aschantin can suppress cell proliferation by inhibiting G_1/S cell cycle transition.

Aschantin selectively inhibits Akt/GSK3β signaling pathway, but not ERKs/RSKs signaling pathway

To determine the aschantin target signaling pathway(s), the phosphoprotein profiles of MAPK and PI3K/Akt signaling pathways were analyzed by western blotting. Aschantin did not affect the EGF-induced phosphorylation of the MEKs, ERKs and RSKs (Figure 2A). These results indicated that aschantin's target was not the MAPK signaling pathway, because EGF did not stimulate the phosphorylation of c-Jun N-terminal kinases and p38 kinases (18). Importantly, EGF-induced Akt phosphorylation at Ser473, a target phosphorylation amino acid by mTORC2 (22), and Thr308, a target phosphorylation amino acid by PI3K (23), were inhibited by aschantin treatment in a dose-dependent manner (Figure 2B). Moreover, the phosphorylation of GSK3β at Ser9 and p70S6K at Thr389 induced by EGF were suppressed by

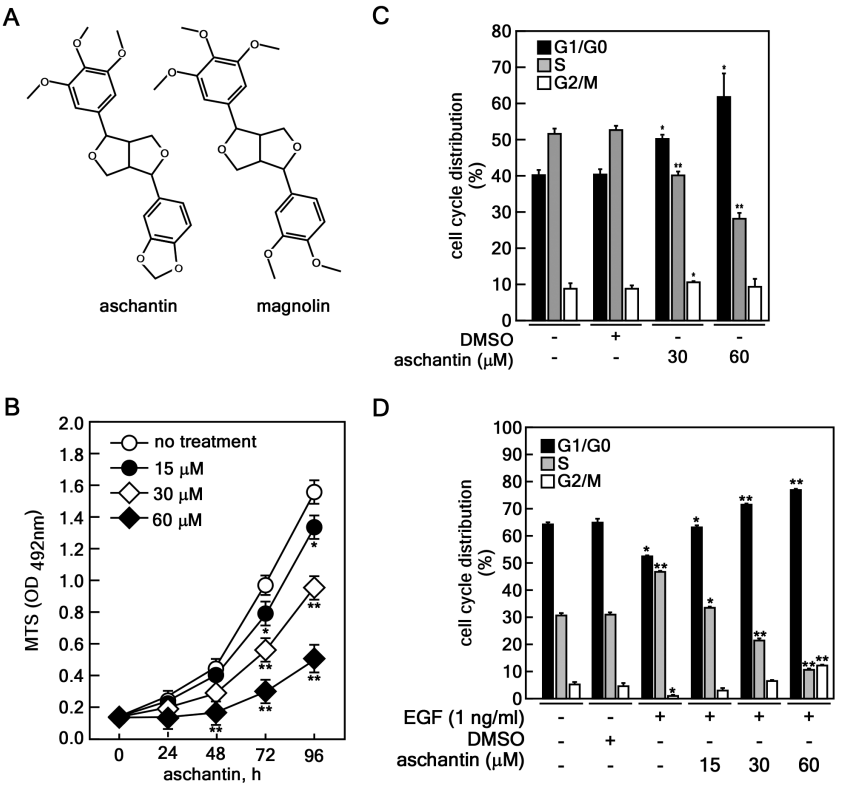

Figure 1. Aschantin suppresses cell proliferation by inhibition of G_1/S cell cycle transition in JB6 Cl41. (**A**) The chemical structures of aschantin and magnolin. (**B**) Aschantin inhibits cell proliferation in JB6 Cl41 cells. JB6 Cl41 cells (1×10^3) were seeded into 96-well cell culture plates and cell proliferation was measured at 24 h intervals over 96 h. (**C**) Aschantin induces G_1/G_0 cell cycle accumulation. JB6 Cl41 cells (2×10^5) were seeded into 60-mm cell culture dishes and cultured overnight. The cells were treated with the indicated doses of aschantin for 12 h, and then cell cycle populations were measured by flow cytometry analysis. (**D**) Aschantin inhibits G_1/S cell cycle transition. JB6 Cl41 cells (2×10^5) were seeded into 60-mm cell culture dishes and cultured overnight. The cells were starved for 24 h supplemented with 0.1% FBS-MEM, pretreated for 30 min with the indicated doses of aschantin and then cotreated with EGF and aschantin as indicated for 12 h. The cell cycle populations were measured by FACS analysis. (B–D) Data are presented the mean ± SD of values from triplicate experiments and statistical significance was determined using the Student's *t*-test (*$P < 0.05$; **, $P < 0.01$).

cotreatment with EGF and aschantin in a dose-dependent manner (Figure 2C). Since GSK3β, a downstream kinase molecule of Akt, plays a key role in regulation of cell proliferation (24), we compared the cell proliferation using GSK3β$^{+/+}$ and GSK3β$^{-/-}$ MEFs. As expected, GSK3β deficiency accelerated cell proliferation compared with GSK3β$^{+/+}$ MEFs (Figure 2D). The same effects were observed by GSK3β knockdown with sh-RNA in JB6 Cl41 cells (Figure 2E). These results indicated that aschantin can selectively inhibit the mTOR/AKT signaling pathway, resulting in inhibition of AKT-mediated cell proliferation.

Aschantin targets the active pocket of mTOR kinase

Inhibition of Akt phosphorylation at Ser473 and Thr308 by aschantin (Figure 2B) suggested that three upstream kinases including PI3K, PDK1 and mTORC2 might be targets of aschantin. To examine this hypothesis, computational docking analyses of aschantin with each crystal structure of PI3K, PDK1 or mTOR were done. The crystal structures of PI3K (3HHM), PDK1 (1JM6) and (4JT6) were obtained from the PDB (http://www.rcsb.org/pdb/home/home.do) and the flexible docking of aschantin with PI3K, PDK1 or mTOR kinase domain was performed by the standard precision mode. Aschantin formed hydrogen bonds with PI3K at Val851, PDK1 at Gly1321 and mTOR at Val2240 (Figure 3A). The docking score of aschantin expressed as free energy (ΔG; kcal/mol) was –5.7, –6.9 and –7.7 against each kinase domain of PI3K, PDK1 and mTOR, respectively (Figure 3B). Although the docking score of mTOR kinase against aschantin was lowest among the three kinases, ΔG did not greatly differ among PI3K, PDK1 and mTOR. Thus, we conducted an *in vitro* kinase assay using each active kinase and each bacterial purified Akt protein. Aschantin dose-dependently inhibited the phosphorylation of Akt at Ser473 when the *in vitro* kinase assay was conducted with active mTOR (Figure 3C). The IC_{50} of aschantin on mTOR kinase activity was ~ 400 nM (Figure 3C). However, aschantin reduced phosphorylation of Akt at Thr308 was not observed in the *in vitro* kinase assay when conducted with active PDK1 (Figure 3D). Moreover, using competition-based p110α activity assay system, we found that PI3K kinase activity was not inhibited by aschantin (Figure 3E). To examine whether aschantin occupied the kinase active pocket of mTOR kinase, we conducted an aschantin competition assay with ATP-conjugated agarose beads. The binding of ATP-bead and mTOR kinase was reduced by addition of aschantin in a dose-dependent manner (Figure 3F). We further hypothesized that the reduction of mTOR kinase activity and ATP-bead binding by aschantin treatment might be caused from the integrity alteration of mTOR complex. To prove the hypothesis, we conducted immunoprecipitation of endogenous mTOR and ectopic expressed Flag-mTOR in the presence or absence of aschantin. The results demonstrated that aschantin treatment did not affect the coimmunoprecipitation of raptor, a specific component of mTORC1 complex, and rictor, a specific component of mTORC2 complex (Figure 3G). Additionally, the kinase profiler assay was carried out using MAP kinase profiler assay kit (Upstate Biotechnology, Lake Placid, NY)

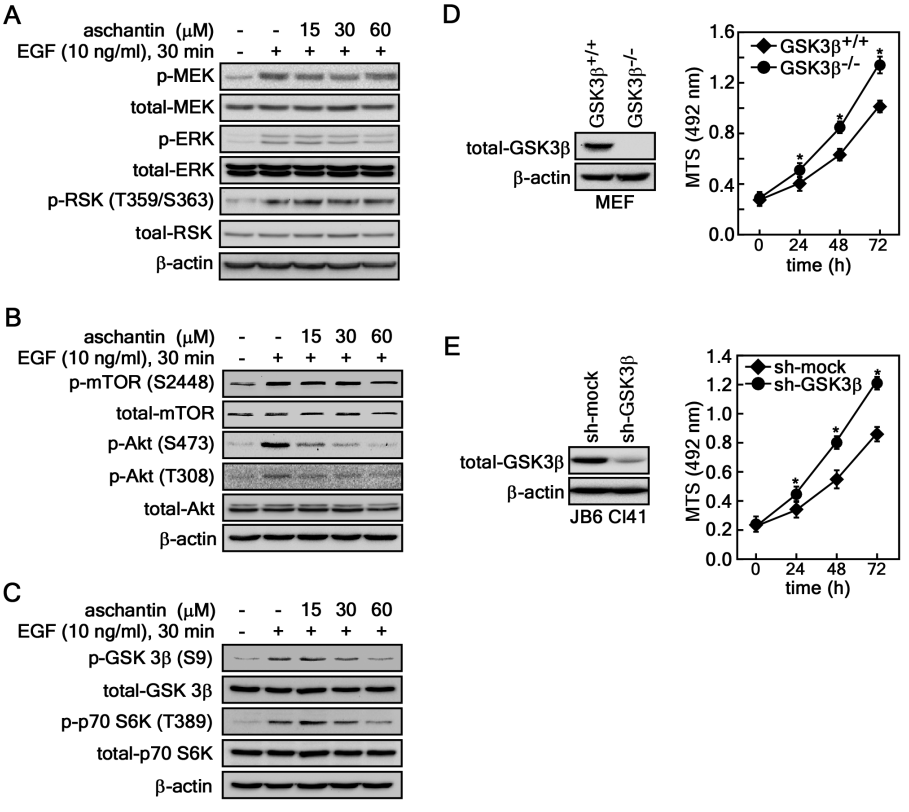

Figure 2. Aschantin selectively inhibits the Akt/GSK3β signaling pathway but not the ERKs/RSKs signaling pathway. (**A**) Aschantin does not affect the MEK/ERK/p90RSK signaling pathway. JB6 Cl41 cells (1×10^6) were seeded in 100-mm cell culture dishes and cultured overnight. The cells were starved for 24 h with 0.1% FBS-MEM, pre-treated with the indicated doses of aschantin for 30 min, and then cotreated with EGF and aschantin for 30 min. The specific proteins were visualized by western blotting using specific antibodies as indicated. (**B**) Aschantin inhibits Akt phosphorylation. The JB6 Cl41 cells were prepared as described in (A). The proteins were extracted, and phosphorylated and total mTOR and Akt were visualized by western blotting using specific antibodies as indicated. (**C**) Aschantin inhibits Akt activity. The JB6 Cl41 cells were prepared as described in (A). The proteins were extracted, and phospho-GSK3β and -p70S6K, and total-GSK3β and -p70S6K were visualized by western blotting using specific antibodies as indicated. (**D**) GSK3β deficiency induces cell proliferation. *Panel*, conformation of GFK3β deficiency by western blotting. GSK3β$^{+/+}$ and GSK3β$^{-/-}$ MEFs were cultured and cell lysates were prepared. GSK3b protein levels were visualized by western blotting using the GSK3b specific antibody. *Graph*, GSK3β$^{+/+}$ and GSK3β$^{-/-}$ MEFs (1×10^3) were seeded into 96-well plates, and cell proliferation was measured at 24 h intervals over 96 h. (**E**) Knockdown of GSK3β induces cell proliferation. *Panel*, pLenti-mock or -shGSK3β was infected into JB6 Cl41 cells and knockdown of GSK3β was visualized by western blotting. *Graph*, knockdown of GSK3β attenuates cell proliferation. The GSK3β knockdown and mock cells (1×10^3) were seeded into 96-well plates and cell proliferation was measured at 24 h intervals over 96 h. (A–D) β-Actin was used for an internal control to verify equal protein loading. (D, E) Data are presented the mean ± SD of values from hexaplicate experiments and statistical significance was determined using the Student's *t*-test (*$P < 0.01$).

including JNK1α1 (JNK1), JNK2α2 (JNK2), MAPK1 (ERK1), MAPK2 (ERK2), MEK1, PKB1 (Akt1), PKBβ (Akt2) and SAPK2α (p38 kinase). The results indicated that 10 μM aschantin suppressed about 30% of MEK1 and 27% of ERK1 (Figure 3H). The other kinases, including JNK1, JNK2, ERK2, Akt1, Akt2 and p38 kinase, were inhibited ≤15% (Figure 3H). These results demonstrated that aschantin targeted the active pocket of mTOR, but not both PI3K and PDK1, and competed with ATP.

Blockage of mTOR/Akt signaling by aschantin suppresses AP-1 transactivation activity through GSK3β-mediated c-Jun destabilization

Oncogenic transcription factors including c-Jun are very unstable proteins due to their short half-life caused by ubiquitination-dependent destabilization (16). Post-translational modifications, such as phosphorylation, plays a key role for instant activity regulation of c-Jun. Phosphorylation of c-Jun at Ser63/73 increases the transactivation activity of c-Jun, which enhances expression of target genes (25). In contrast, the phosphorylation status of c-Jun at Ser243, Ser249 and Thr231 is inversely corelated with the phosphorylation-dependent c-Jun transactivation activity (26,27) and protein stability (28). GSK3β plays an important role in phosphorylation of c-Jun at Ser243, which is needed for Fbxw-7 recognition and ubiquitination (16). Aschantin inhibited AP-1 transactivation activity (Figure 4A). c-Jun phosphorylation at Ser63/73 and total-c-Jun levels were decreased by aschantin treatment (Figure 4B). Moreover, phosphorylation of c-Jun at Ser243 was increased by aschantin treatment (Figure 4B). These results suggested that decreased c-Jun protein level by aschantin treatment might be attributed to c-Jun protein destabilization. Real-time PCR analysis confirmed that decreased c-Jun protein level by aschantin was not due to the alteration of *c-jun* mRNA expression (Figure 4C). Thus, we conducted a rescue experiment using MG132, a proteasome inhibitor. Increased phospho- and total-c-Jun protein levels by EGF stimulation were suppressed by cotreatment with EGF and aschantin (Figure 4D). Importantly, decreased phospho- and total-c-Jun protein levels caused by aschantin treatment were rescued by MG132 treatment (Figure 4D). To examine whether reduced total c-Jun protein level by aschantin was ubiquitin-dependent, we transiently transfected with *pHA*-ubiquitin, and then cotreated with MG132 and aschantin. Ubiquitination of c-Jun was increased by aschantin treatment in a dose-dependent manner (Figure 4E). Moreover, an immunocytofluorescence assay confirmed that EGF-induced

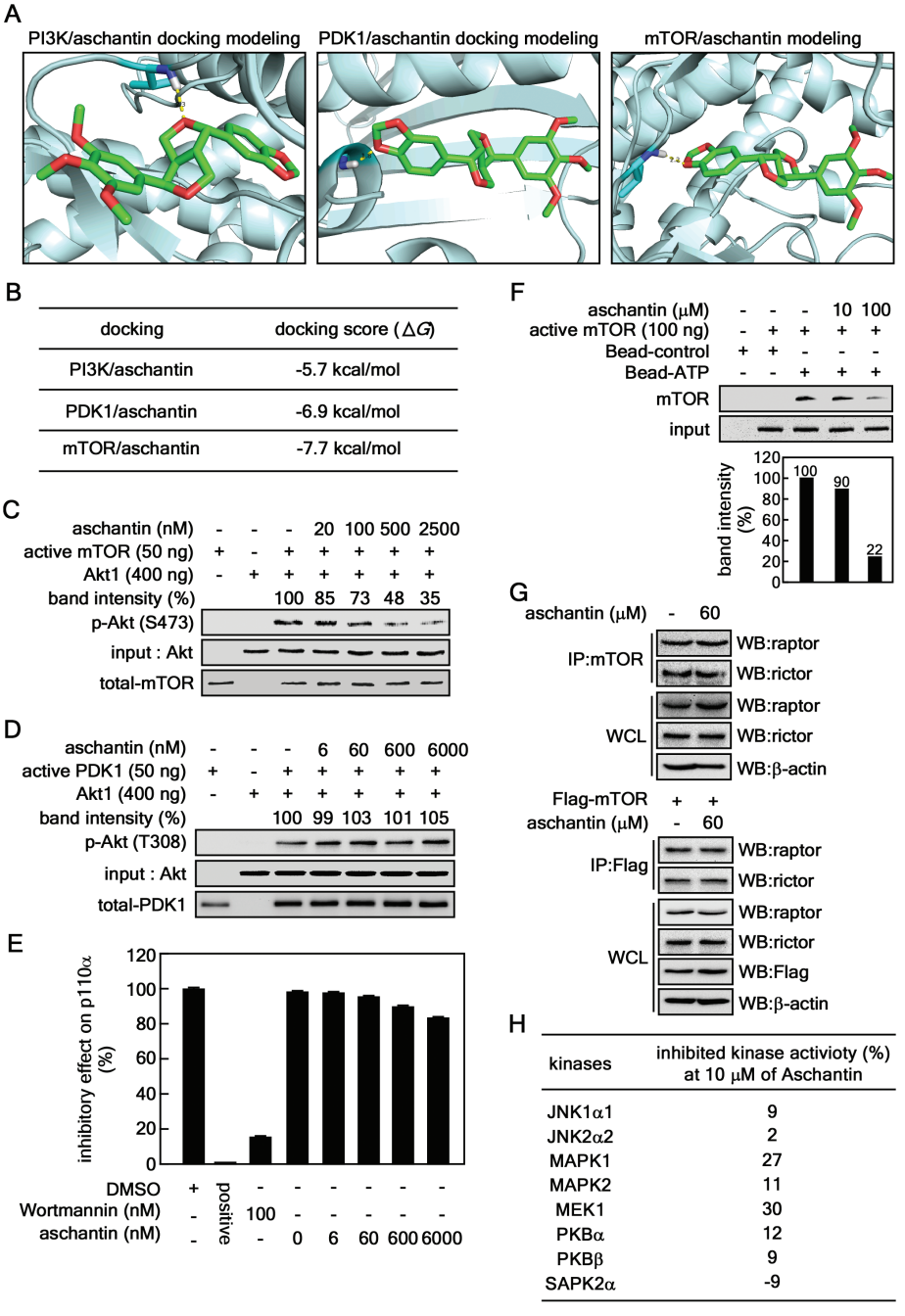

Figure 3. Aschantin targets mTOR kinase. (**A**) Supercomputational docking analysis of aschantin. Computational docking of aschantin onto each active pocket of 4JT6 (mTor), 3HHM (PI3K) and 1JM6 (PDK1) obtained from Protein Data Bank, PDB. The crystal structure was prepared using the Protein Preparation Wizard in Maestro v9.4. Hydrogens were added consistent with a pH 7.0. All water molecules were removed, and then the structures were minimized with an root mean square deviation cutoff value of 0.3 Å. The program Glide v5.9 was used for ligand docking. The receptor grid was created with the centroid of the crystal ligand as the center of the grid. Flexible docking was performed with extra precision mode. Number of poses per ligand was set to 10 in post-docking minimization and at most one pose would be output. The other parameters were kept as default. (**B**) Docking score obtained from (A). (**C**) Effectiveness of aschantin on the mTOR kinase activity. Active mTOR (50 ng), Akt1 protein (400 ng) and ATP (100 μM of final concentration) were combined with indicated doses of aschantin in 20 μl of reaction mixture, and the reaction was carried out at 30°C for 30 min. The phosphorylated Akt at Ser473 was visualized by western blotting with a specific antibody as indicated. (**D**) Effectiveness of aschantin on the PDK1 activity. Active PDK1 (50 ng), Akt1 protein (400 ng) and ATP (100 μM of final concentration) were combined with indicated doses of aschantin in 20 μl of reaction mixture, and the reaction was carried out at 30 °C for 30 min. The phosphorylated Akt at Thr308 was visualized by western blotting using a specific antibody as indicated. (**E**) Effectiveness of aschantin on the PI3K activity. PI3K inhibitor assay was conducted described in Materials and Methods. (**F**) Aschantin competes with ATP in the active pocket of mTOR kinase. Active mTOR protein (100 ng) was combined with ATP-conjugated beads, washed and then competed with indicated doses of aschantin. The beads were washed and remaining mTOR onto the ATP-bead was visualized by western blotting with an mTOR specific antibody. The band density of mTOR was measured by Image J (ver. 1.37v) computer program. (**G**) Aschantin did not affect the integrity of mTOR complex. Cell lysates extracted from HEK293T cells and HEK293T cells overexpressing Flag-mTOR in the presence or absence of aschantin were utilized for immunoprecipitation using mTOR kinase-specific and Flag-specific antibodies, respectively. Immunoprecipitated mTOR kinases were visualized by western blotting using raptor- or rictor-specific antibody as indicated. β-Actin was used for an internal control to verify equal protein loading. (**H**) Pleiotropic effectiveness of aschantin. The specificity of aschantin was analyzed through KinaseProfiler™ Service (EMD Millipore) with 10 μM of aschantin and kinase substrates. The indicated number is the percentage of inhibited kinase activity.

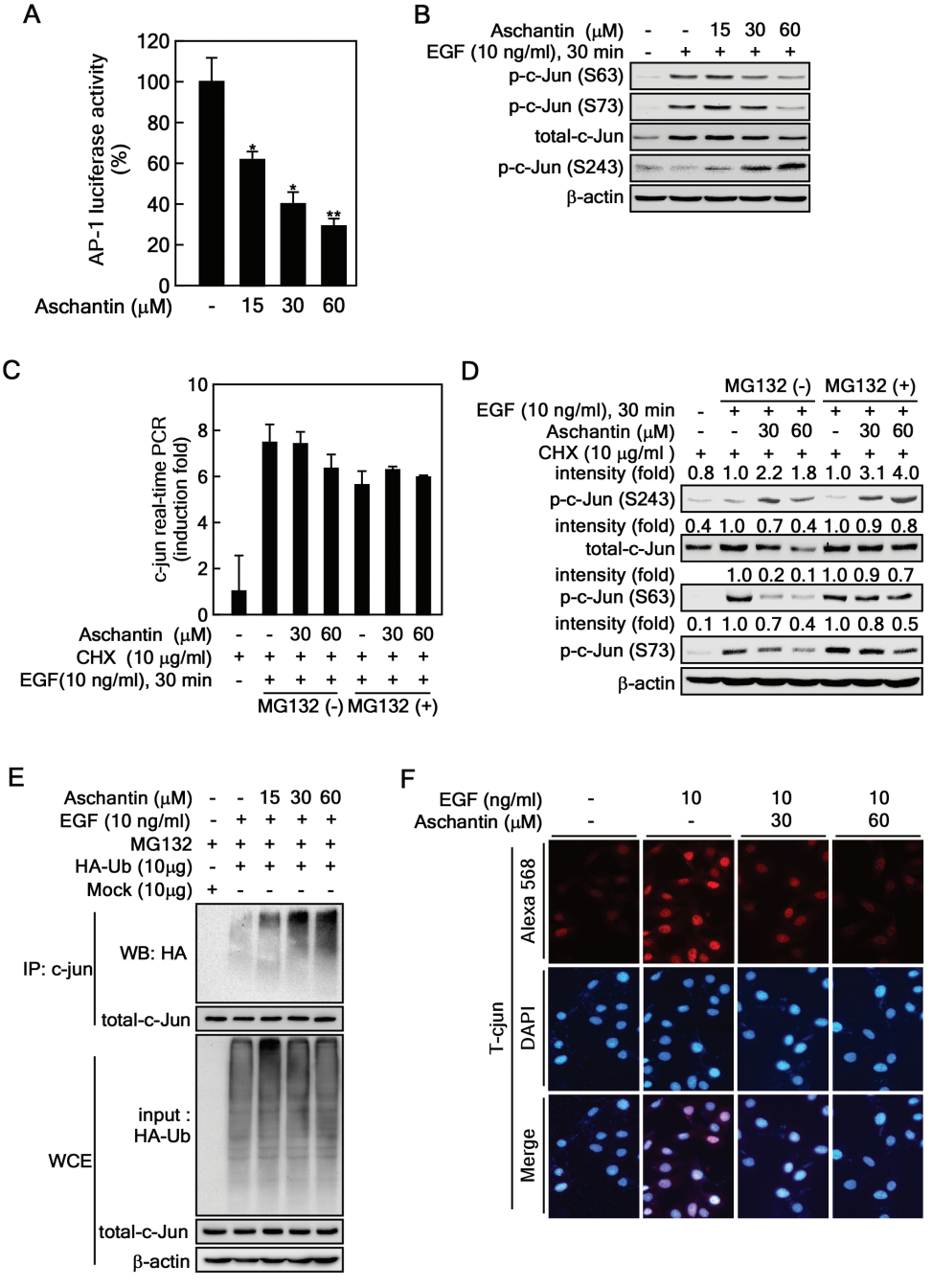

Figure 4. Aschantin decreases c-jun stability by ubiquitination. (**A**) Aschantin suppresses AP-1 transactivation activity. JB6 Cl41 (2×10^4) cells stably transfected with AP-1 luciferase reporter plasmid were seeded into 24-well plates and cultured for 24 h. The cells were starved overnight, pretreated with indicated doses of aschantin for 30 min and cotreated EGF and aschantin as indicated for 12 h. Firefly luciferase activity was measured as described in Materials and Methods. Data are presented the mean ± SD of values from triplicate experiments and statistical significance was determined using the Student's t-test (*$P < 0.05$; **$P < 0.01$). (**B**) Aschantin-mediated alteration of phospho- and total-c-Jun protein levels. JB6 Cl41 cells (1×10^6) were seeded in 100-mm cell culture dishes and cultured overnight. The cells were starved for 24 h with 0.1% FBS-MEM, pretreated with the indicated doses of aschantin for 30 min, and then cotreated with EGF and aschantin for 30 min. The proteins were extracted and visualized by western blotting using specific antibodies as indicated. (**C**) Aschantin does not alter *c-jun* mRNA expression. JB6 Cl41 cells (2×10^5) were seeded in 60-mm cell culture dishes and cultured overnight. The cells were starved for 24 h with 0.1% FBS-MEM and cotreated with cycloheximide (CHX), MG132 (10 μM), EGF and aschantin as indicated for 30 min. The cells were harvested and total RNAs were extracted using Trizol Reagent. The *c-jun* gene expression was analyzed by real-time PCR using a *c-jun* specific real-time primer set. (**D**) Aschantin induces c-Jun destabilization through the proteasomal degradation pathway. The JB6 Cl41 cells were prepared as described in (C) The specific proteins were visualized by western blotting using specific antibodies as indicated. (**E**) Aschantin induces c-Jun ubiquitination. JB6 Cl41 cells (1×10^6) were seeded in 100-mm cell culture dishes, transfected with HA-mock or HA-ubiquitin expression vector, and cultured for 24 h. The transfected cells were treated with indicated doses of aschantin and MG132 (10 μM) for 6 h. The total-c-Jun protein was immunoprecipitated and ubiquitin-conjugated c-Jun protein levels were visualized by western blotting using specific antibodies as indicated. (**F**) Aschantin inhibited nuclear accumulation of c-Jun. JB6 Cl41 (2×10^4) cells seeded in four-chamber slide and cultured overnight. The cells were starved overnight, pretreated aschantin for 30 min and cotreated with EGF and aschantin for 30 min as indicated. The cells were fixed and permeabilized, and total c-Jun protein level was visualized using a c-Jun antibody and Alexa 568 conjugated secondary antibody. The fluorescence was observed under confocal microscope (×400). DAPI was used for nuclear staining. (B, D and E) β-Actin was used for an internal control to verify equal protein loading.

total c-Jun protein level in the nucleus was decreased by aschantin treatment in a dose-dependent manner (Figure 4F). These results demonstrated that aschantin decreases c-Jun stability through ubiquitination dependent proteasomal degradation pathway.

Aschantin inhibits EGF-induced cell transformation

After activation, Akt is able to translocate to the nucleus and phosphorylate downstream transcription factors including CREB (29), E2F (30), NF-κB (31) and FOXO (32). Akt is often upregulated in cancer cells by constitutive active PI3K mutation (33). Moreover, upregulation of *Akt* gene expression and activity increases the phosphorylation of mTOR signaling molecules including p70S6K and 4E-BP1, which has been associated with the pathology of pancreatic, glioma and prostate cancers (33,34). Previously, we demonstrated that c-Jun has a key role in EGF-induced cell transformation (18). Presently, aschantin suppressed AP-1 transactivation activity by reducing c-Jun stability through the ubiquitination-dependent proteasomal degradation pathway (Figure 4). Thus, we conducted an anchorage-independent cell transformation assay induced by EGF using JB6 Cl41 and HaCaT premalignant human skin keratinocytes. Aschantin inhibited anchorage-independent cell transformation in both JB6 Cl41 and HaCaT cells (Figure 5A and B and Supplementary Figure 3A and B, available at *Carcinogenesis* Online). Especially, 60 μM aschantin suppressed the cell transformation ~90% (Figure 5A and B and Supplementary Figure 3A and B, available at *Carcinogenesis* Online). To confirm whether knockdown of mTOR showed similar effects as aschantin, mTOR knockdown HaCaT cells were generated (Figure 5C) and used to confirm that EGF-induced cell transformation was totally abrogated by mTOR knockdown (Figure 5D). Additionally, ATP-competitive mTOR kinase inhibitor also suppressed EGF-induced cell transformation of JB6 Cl41 and HaCaT cells (Supplementary Figure 4, available at *Carcinogenesis* Online). These results demonstrated that aschantin is a natural compound targeting mTOR kinase domain and that it suppresses cell proliferation and transformation induced by tumor promoters such as EGF. The results further indicate the potential of aschantin as a natural chemoprevention and cancer therapeutic compound.

Aschantin suppresses anchorage-independent colony growth of cancer cells

To examine the aschantin effect in cancer cells, phospho- and total-mTOR protein levels were analyzed in pancreatic cancer

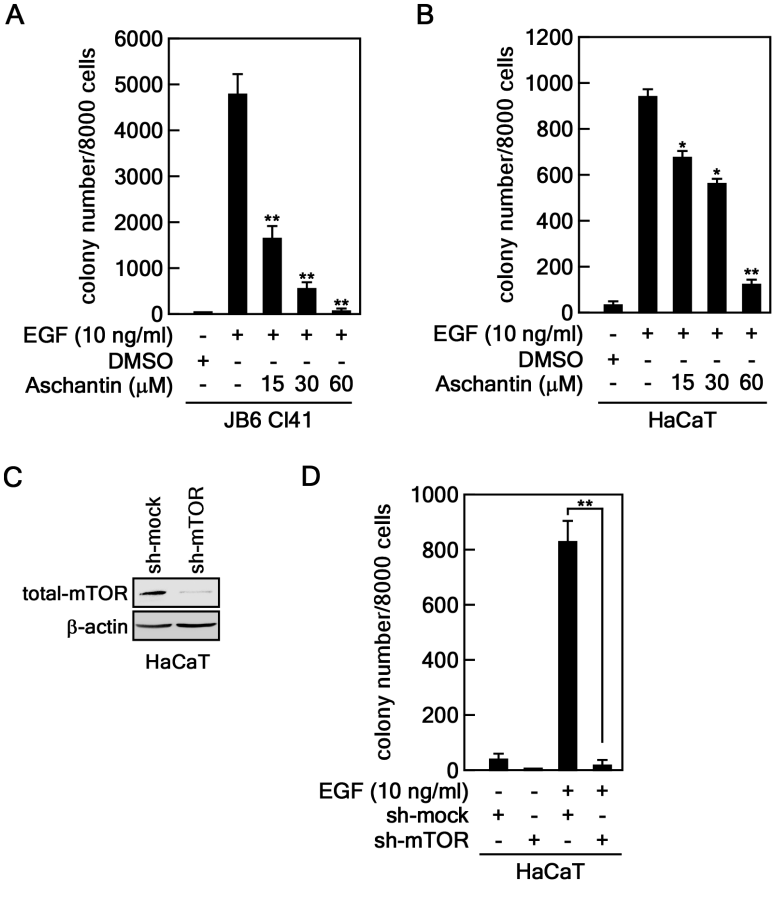

Figure 5. Aschantin suppresses EGF-induced neoplastic cell transformation. (**A**) Aschantin inhibits EGF-induced cell transformation in JB6 Cl41 cells. JB6 Cl41 cells (8×10^3) were exposed to EGF (10 ng/ml) and aschantin in 1 ml of 0.3% BME agar containing 10% FBS as indicated. The cultures were maintained in a 37°C, 5% CO_2 incubator for 14 days, and then colonies were counted using an ECLIPSE Ti inverted microscope and the NIS-Elements AR (V. 4.0) computer software program. (**B**) Aschantin inhibits EGF-induced cell transformation in HaCaT cells. HaCaT cells (8×10^3) were exposed to EGF (10 ng/ml) and aschantin in 1 ml of 0.3% BME agar containing 10% FBS as indicated. The cultures were maintained in a 37°C, 5% CO_2 incubator for 21 days, and then colonies were counted using an ECLIPSE Ti inverted microscope and the NIS-Elements AR (V. 4.0) computer software program. (**C**) Knockdown of mTOR in HaCaT. The pLenti-mock or -sh-mTOR lenti-viral vector was infected into HaCaT cells and knockdown of mTOR was visualized by western blotting. (**D**) Knockdown of mTOR suppresses EGF-induced cell transformation in HaCaT cells. HaCaT cells stably expressing mock or sh-mTOR (8×10^3) were exposed to EGF (10 ng/ml) in 1 ml of 0.3% BME agar containing 10% FBS as indicated. The cultures were maintained in a 37°C, 5% CO_2 incubator for 21 days, and colonies were counted using an ECLIPSE Ti inverted microscope and the NIS-Elements AR (V. 4.0) computer software program. (A, B and D) Data are presented as mean ± SD of values from triplicate experiments and statistical significance was determined using the Student's *t*-test (*$P < 0.05$; **$P < 0.01$).

cells (MIAPaCa-2, AsPC-1 and BxPC-3) and prostate cancer cells (DU-145 and LNCaP). Phospho-mTOR at Ser2448 and total protein levels were prominently detected in MIAPaCa-2 and LNCaP cells (Figure 6A). Next, we examined the efficacy of aschantin in inhibiting colony growth in soft agar. Aschantin inhibited colony growth of MIAPaCa-2 and LNCaP cells in a dose-dependent manner. In particular, 15 μM aschantin suppressed ~90% of LNCaP cell colony growth in soft agar (Figure 6B, and Supplementary Figure 6A and B, available at *Carcinogenesis* Online). These inhibitory effects were also observed by knocking down mTOR in MAIPaCa-2 and LNCaP cells (Figure 6C, and Supplementary Figures 5A and B, 6C and D, available at *Carcinogenesis* Online). Moreover, aschantin suppressed phospho-c-Jun Ser63/73 and total-c-Jun protein levels in LNCaP cells (Figure 6D). The decreased c-Jun protein levels were corelated with the phosphorylation of GSK3β at Ser9 and c-Jun at Ser243 in LNCaP cells (Figure 6D) as well as in JB6 Cl41 cells (Figures 2C and 4B), resulting in inhibition of AP-1 transactivation activity (Figure 6E). ATP competitive inhibitor of mTOR kinase decreased protein levels of phospho-Akt at Ser473 and total-c-Jun (Figure 6F). Moreover, real-time PCR analysis demonstrated that the decreased total-c-Jun protein level and AP-1 luciferase activity were not caused by the suppression of c-Jun mRNA expression in LNCaP cells (Figure 6G). Importantly, ubiquitinated c-Jun proteins were increased by aschantin treatment in a dose dependent manner in LNCaP cells (Figure 6H). Taken together, these results demonstrate that aschantin can inhibit cell proliferation and transformation induced by EGF in non-malignant JB6 Cl41 and HaCaT cells, and suppress cell proliferation and colony growth in human cancer cells, such as MIAPaCa-2 and LNCaP cells, in soft agar.

Discussion

Activation of Akt, a serine–threonine kinase located downstream of PTEN/PI3K, stimulates cell cycle progression, survival and migration through phosphorylation and activation of diverse physiological substrates (35). Akt activity is upregulated by PTEN/PI3K/PDK1 signaling (36), and mTORC2, a rictor-containing mTOR complex that phosphorylates Akt at Ser473 (37). mTORC1 is a downstream serine/threonine kinase protein that transduces the activated Akt signal to p70S6K and 4E-BP1 (33,34). One of the most important facets of mTORC1 and mTORC2 is that these two complexes share the same kinase. Although rapamycin inhibits the phosphorylation of 4E-BP1, rapamycin treatment induces activity of mTORC2 via a negative-feedback regulation loop, resulting in activation of Akt by its phosphorylation at Ser473 (4,38). Presently, aschantin was demonstrated to target an active site of mTOR kinase domain and compete with ATP (Figure 3). In cell culture experiments, EGF-induced Akt phosphorylation at both Ser473 and Thr308 was inhibited by aschantin (Figure 2B). The inhibition of Akt phosphorylation activated GSK3β kinase activity by suppression of GSK3β phosphorylation at Ser9 (Figure 2C). The activated GSK3β phosphorylated c-Jun at Ser243, which can serve as a docking site for the Fbxw7 E3 ubiquitin ligase, resulted in increased protein destabilization (16). Total c-Jun protein levels were increased by EGF and decreased by cotreatment with EGF and aschantin (Figure 4B) without alteration of mRNA expression (Figure 4C). Importantly, ubiquitination of c-Jun was increased by aschantin treatment (Figure 4E), and MG-132 treatment rescued phospho- and total-c-Jun protein levels (Figure 4D). Based on these data, we conclude that aschantin can inhibit activities of both mTORC1 and mTORC2.

Aschantin is a lignan compound that modulates nitric oxide production-related gene expression, which is mainly regulated by NF-κB and AP-1 transactivation activity (39,40). Since natural compounds generally tend to bind with multiple proteins, we confirmed that the specific activity of aschantin on the inhibition of cell proliferation, cell transformation and cancer cell growth was from the inhibition of mTOR kinase (Figure 3). Although 10 μM aschantin inhibited ~30% of MEK1 activity, 400 nM aschantin caused ~50% inhibition of Akt phosphorylation at Ser473 (Figure 3C). Importantly, aschantin suppressed anchorage-independent colony growth of MIAPaCa-2 pancreatic and LNCaP prostate cancer cells (Figure 6B). The inhibitory molecular mechanism of aschantin was mediated through the ubiquitination-mediated c-Jun destabilization (Figure 6H). The data were very consistent with the results obtained by the knockdown of mTOR using short hairpin-RNA and by the inhibition of mTOR kinase using ATP-competitive inhibitor AZD8055 (Figure 6C and F). These results strongly suggest that aschantin may have the potential to treat human cancers.

c-Jun is the normal cellular counterpart of the viral Jun oncoprotein (c-Jun) encoded by an avian sarcoma virus (ASV17) (41). c-Jun transcriptional activity is increased by exposing cells to phorbol esters, growth factors, such as EGF, and transforming oncogenes like Ras (42). Phosphorylation of c-Jun at Ser63/73 by environmental stimuli, such as ultraviolet light, cytokines or growth factors, stimulates c-Jun/AP-1 activity (43) through different signaling pathways, including ERKs (43) and c-Jun N-terminal kinases (JNKs) (44). Although activity regulation of c-Jun by transient modification is important in the response to the environment, protein stability of c-Jun is important in cellular c-Jun functions including cell proliferation and transformation. The GSK3β signaling pathway regulated by PI3K/Akt signaling mediates phosphorylation of c-Jun in its DNA binding domain, resulting in interruption of DNA binding affinity and transactivation of c-Jun (16). Aschantin induced c-Jun ubiquitination and inhibited c-Jun/AP-1 luciferase activity (Figure 4).

Since the PI3K signaling pathway is key in cell proliferation and survival as shown in Ras signaling pathway, the PI3K/AktT/mTOR signaling axis has been especially interesting in the development of cancer therapeutic drugs (45). Although the cells harboring constitutively active mutations in PI3K signaling pathway affects its sensitivity to EGFR inhibitors, the mechanism is less clearly understood. Moreover, constitutively active PI3K mutations within the exon 20, an encoding kinase domain, confer intrinsic resistance to EGFR-targeted antibodies (46). Loss of PTEN function induces activation of PI3K pathway and has been linked to intrinsic resistance to EGFR-targeted antibodies (47). Activated PI3K signal is transduced to mTOR through Akt, and then expressed in diverse cellular responses including cancer development. Thus, wortmannin, an irreversible PI3K inhibitor (48), and LY294002, a reversible and ATP-competitive PI3K inhibitor (49), have been used as research tools for more a decade in the biology of human cancer. Rapamycin was developed to prevent rejection in organ transplant patients and act as an allosteric mTORC1 inhibitor without directly affecting the mTOR catalytic site (50). Rapamycin sensitivity is associated with the inactivation mutation of PTEN, constitutively active mutation of PI3K and hyperactivation of Akt (33). However, rapamycin resistance is also associated with KRAS or BRAF mutations (22). Furthermore, predominant mTORC1 inhibition by rapamycin induces Akt activation by phosphorylation at Ser473 (4). Thus, while rapamycin predominantly inhibits mTORC1, mTOR kinase inhibitors have advantages over rapamycin as mTOR inhibitors, resulting in inhibition of both mTORC1 and mTORC2.

Our results demonstrate that aschantin inhibits mTOR kinase activity by competing with ATP. Taken together, aschantin

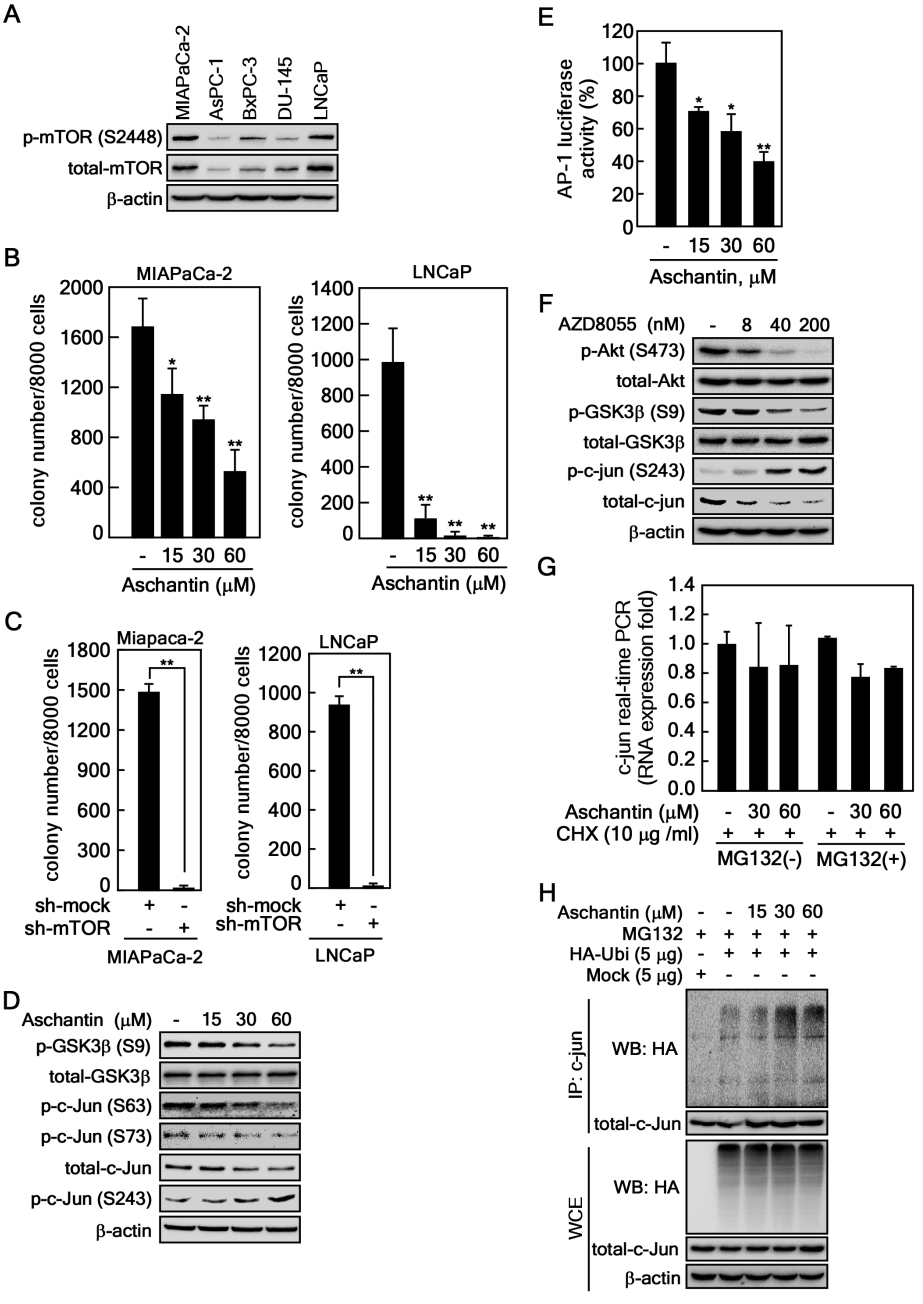

Figure 6. Aschantin inhibits cancer cell growth by induction of c-Jun destabilization. (**A**) mTOR protein levels in various cancer cells. Pancreatic and prostate cancer cells as indicated were cultured with appropriate complete culture medium. The proteins were extracted and phospho- and total-mTOR proteins were visualized by western blotting. (**B**) Aschantin inhibits colony growth of MIAPaCa-2 and LNCaP cells in soft agar. MIAPaCa-2 and LNCaP cells (8×10^3) were exposed to indicated doses of aschantin in 1 ml of 0.3% BME agar containing 10% FBS. The cultures were maintained in a 37°C, 5% CO_2 incubator for 21 days, and then colonies were counted using an ECLIPSE Ti inverted microscope and the NIS-Elements AR (V. 4.0) computer software program. (**C**) Knockdown of mTOR suppresses colony growth in soft agar in LNCaP cells. MIAPaCa-2 and LNCaP cells (8×10^3) stably expressing pLenti-mock or -sh-mTOR were exposed to indicated doses of aschantin in 1 ml of 0.3% BME agar containing 10% FBS. The cultures were maintained in a 37°C, 5% CO_2 incubator for 21 days, and then colonies were counted using an ECLIPSE Ti inverted microscope and the NIS-Elements AR (V. 4.0) computer software program. (**D**) Aschantin modulates Akt-mediated signaling in LNCaP cells. LNCaP cells (1×10^6) were seeded into 100-mm culture dishes and treated with aschantin as indicated. The protein was extracted and specific protein levels were visualized by western blotting as indicated. (**E**) Aschantin inhibits AP-1 transactivation activity in LNCaP cells. LNCaP (2×10^4) cells stably transfected with AP-1 luciferase reporter plasmid were seeded into 24-well plates and cultured for 24 h. The cells were treated with indicated doses of aschantin for 12 h. Firefly luciferase activity was measured as described in Materials and Methods. (**F**) ATP-competitive inhibitor of mTOR suppresses the protein levels of phospho-Akt at Ser473 and total-c-Jun. LNCaP cells (1×10^6) were seeded into 100-mm culture dishes and treated with AZD8055 as indicated. The protein was extracted and phospho- and -total Akt and total-c-Jun protein were visualized by western blotting. (**G**) Aschantin does not alter *c-jun* mRNA expression in LNCaP cells. LNCaP cells (2×10^5) were seeded in 60-mm cell culture dishes and cultured overnight. The cells were treated with cycloheximide (CHX) either presence of MG132 (10 μM) or not for for 30min. The cells were harvested, and total RNAs were extracted using Trizol Reagent. The *c-jun* gene expression was analyzed by real-time PCR using a *c-jun* specific real-time primer set. (**H**) Aschantin induces c-Jun ubiquitination in LNCaP cells. LNCaP cells (1×10^6) were seeded in 100-mm cell culture dishes, transfected with HA-mock or HA-ubiquitin expression vector, and cultured for 24 h. The transfected cells were treated with indicated doses of aschantin and MG132 (10 μM) for 6 h. The endogenous c-Jun protein was immunoprecipitated and ubiquitin-conjugated c-Jun protein level was visualized by Western blotting using specific antibodies as indicated. (A, D, E and F) β-Actin was used for an internal control to verify equal protein loading. (B, C and E) Data are presented the mean ± SD of values from triplicate experiments and statistical significance was determined using the Student's *t*-test (*$P < 0.05$; **$P < 0.01$).

is a natural compound targeting mTOR kinase domain with an IC_{50} of ~400 nM, and is a potentially valuable chemopreventative or therapeutic agent.

Supplementary material

Supplementary Materials and Methods and Figures 1–6 can be found at http://carcin.oxfordjournals.org/

Funding

This study was supported by the Research Fund, M-2012-B0002-00028 of The Catholic University of Korea, by Basic Science Research Program through the National Research Foundation of Korea (NRF) funded by the Ministry of Education, Science and Technology (2012R1A1A2000961), by a grant from KRIBB Initiative Program (KGM1221313) and by the Ministry of Science, ICT and Future Planning (2012M3A9B6055466 and NRF-2014R1A2A11050004).
Conflict of interest statement: None declared.

References

1. Guertin, D.A. et al. (2007) Defining the role of mTOR in cancer. Cancer Cell, 12, 9–22.
2. Lindsley, J.E. et al. (2004) Nutrient sensing and metabolic decisions. Comp. Biochem. Physiol. B. Biochem. Mol. Biol., 139, 543–559.
3. Sarbassov, D.D. et al. (2005) Growing roles for the mTOR pathway. Curr. Opin. Cell Biol., 17, 596–603.
4. O'Reilly, K.E. et al. (2006) mTOR inhibition induces upstream receptor tyrosine kinase signaling and activates Akt. Cancer Res., 66, 1500–1508.
5. Chresta, C.M. et al. (2010) AZD8055 is a potent, selective, and orally bioavailable ATP-competitive mammalian target of rapamycin kinase inhibitor with *in vitro* and *in vivo* antitumor activity. Cancer Res., 70, 288–298.
6. Thoreen, C.C. et al. (2009) An ATP-competitive mammalian target of rapamycin inhibitor reveals rapamycin-resistant functions of mTORC1. J. Biol. Chem., 284, 8023–8032.
7. Janes, M.R. et al. (2010) Effective and selective targeting of leukemia cells using a TORC1/2 kinase inhibitor. Nat. Med., 16, 205–213.
8. Zoncu, R. et al. (2011) mTOR: from growth signal integration to cancer, diabetes and ageing. Nat. Rev. Mol. Cell Biol., 12, 21–35.
9. Fan, Q.W. et al. (2006) A dual PI3 kinase/mTOR inhibitor reveals emergent efficacy in glioma. Cancer Cell, 9, 341–349.
10. Liu, T.J. et al. (2009) NVP-BEZ235, a novel dual phosphatidylinositol 3-kinase/mammalian target of rapamycin inhibitor, elicits multifaceted antitumor activities in human gliomas. Mol. Cancer Ther., 8, 2204–2210.
11. Huang, C. et al. (1998) Shortage of mitogen-activated protein kinase is responsible for resistance to AP-1 transactivation and transformation in mouse JB6 cells. Proc. Natl. Acad. Sci. USA, 95, 156–161.
12. Bode, A.M. et al. (2003) Mitogen-activated protein kinase activation in UV-induced signal transduction. Sci. STKE, 2003, RE2.
13. Liu, K. et al. (2011) Eriodictyol inhibits RSK2-ATF1 signaling and suppresses EGF-induced neoplastic cell transformation. J. Biol. Chem., 286, 2057–2066.
14. Maeno, K. et al. (2006) Altered regulation of c-jun and its involvement in anchorage-independent growth of human lung cancers. Oncogene, 25, 271–277.
15. Cho, Y.Y. et al. (2009) Cyclin-dependent kinase-3-mediated c-Jun phosphorylation at Ser63 and Ser73 enhances cell transformation. Cancer Res., 69, 272–281.
16. Wei, W. et al. (2005) The v-Jun point mutation allows c-Jun to escape GSK3-dependent recognition and destruction by the Fbw7 ubiquitin ligase. Cancer Cell, 8, 25–33.
17. Shen, Y. et al. (2008) Inhibitions of mast cell-derived histamine release by different Flos Magnoliae species in rat peritoneal mast cells. Phytomedicine, 15, 808–814.
18. Lee, C.J. et al. (2013) Targeting of magnolin on ERKs inhibits Ras/ERKs/RSK2-signaling-mediated neoplastic cell transformation. Carcinogenesis.
19. Lee, H.K. et al. (2002) New Lignans Isolated From Magnolia flos with Leukotriene Synthesis Inhibitory Activity. Korea Intellectual Property Offcie, Korea Patent # 10-0321313-0000. Korea Institute of Science & Technology, Korea.
20. Colburn, N.H. et al. (1981) Dissociation of mitogenesis and late-stage promotion of tumor cell phenotype by phorbol esters: mitogen-resistant variants are sensitive to promotion. Proc. Natl. Acad. Sci. USA, 78, 6912–6916.
21. Jun, A.Y. et al. (2012) Extract of Magnoliae Flos inhibits ovariectomy-induced osteoporosis by blocking osteoclastogenesis and reducing osteoclast-mediated bone resorption. Fitoterapia, 83, 1523–1531.
22. Memmott, R.M. et al. (2009) Akt-dependent and -independent mechanisms of mTOR regulation in cancer. Cell. Signal., 21, 656–664.
23. Sarbassov, D.D. et al. (2005) Phosphorylation and regulation of Akt/PKB by the rictor-mTOR complex. Science, 307, 1098–1101.
24. Lee, C.J. et al. (2013) RSK2-induced stress tolerance enhances cell survival signals mediated by inhibition of GSK3β activity. Biochem. Biophys. Res. Commun., 440, 112–118.
25. Smeal, T. et al. (1992) Oncoprotein-mediated signalling cascade stimulates c-Jun activity by phosphorylation of serines 63 and 73. Mol. Cell. Biol., 12, 3507–3513.
26. Woodgett, J.R. et al. (1993) Regulation of jun/AP-1 oncoproteins by protein phosphorylation. Adv. Second Messenger Phosphoprotein Res., 28, 261–269.
27. Srinivas, S. et al. (1994) Polyomavirus middle-sized tumor antigen modulates c-Jun phosphorylation and transcriptional activity. Proc. Natl. Acad. Sci. USA, 91, 10064–10068.
28. Morton, S. et al. (2003) A reinvestigation of the multisite phosphorylation of the transcription factor c-Jun. EMBO J., 22, 3876–3886.
29. Du, K. et al. (1998) CREB is a regulatory target for the protein kinase Akt/PKB. J. Biol. Chem., 273, 32377–32379.
30. Brennan, P. et al. (1997) Phosphatidylinositol 3-kinase couples the interleukin-2 receptor to the cell cycle regulator E2F. Immunity, 7, 679–689.
31. Kane, L.P. et al. (1999) Induction of NF-kappaB by the Akt/PKB kinase. Curr. Biol., 9, 601–604.
32. Buitenhuis, M. et al. (2009) The role of the PI3K-PKB signaling module in regulation of hematopoiesis. Cell Cycle, 8, 560–566.
33. McCubrey, J.A. et al. (2012) Mutations and deregulation of Ras/Raf/MEK/ERK and PI3K/PTEN/Akt/mTOR cascades which alter therapy response. Oncotarget, 3, 954–987.
34. Chow, S. et al. (2006) Constitutive phosphorylation of the S6 ribosomal protein via mTOR and ERK signaling in the peripheral blasts of acute leukemia patients. Exp. Hematol., 34, 1183–1191.
35. Vivanco, I. et al. (2002) The phosphatidylinositol 3-Kinase AKT pathway in human cancer. Nat. Rev. Cancer, 2, 489–501.
36. Myers, M.P. et al. (1998) The lipid phosphatase activity of PTEN is critical for its tumor supressor function. Proc. Natl. Acad. Sci. USA, 95, 13513–13518.
37. Sarbassov, D.D. et al. (2005) Phosphorylation and regulation of Akt/PKB by the rictor-mTOR complex. Science, 307, 1098–1101.
38. Shi, Y. et al. (2005) Mammalian target of rapamycin inhibitors activate the AKT kinase in multiple myeloma cells by up-regulating the insulin-like growth factor receptor/insulin receptor substrate-1/phosphatidylinositol 3-kinase cascade. Mol. Cancer Ther., 4, 1533–1540.
39. Petrova, T.V. et al. (1999) Cyclopentenone prostaglandins suppress activation of microglia: down-regulation of inducible nitric-oxide synthase by 15-deoxy-Delta12,14-prostaglandin J2. Proc. Natl. Acad. Sci. USA, 96, 4668–4673.
40. Zingarelli, B. et al. (2002) Absence of inducible nitric oxide synthase modulates early reperfusion-induced NF-kappaB and AP-1 activation and enhances myocardial damage. FASEB J., 16, 327–342.
41. Maki, Y. et al. (1987) Avian sarcoma virus 17 carries the jun oncogene. Proc. Natl. Acad. Sci. USA, 84, 2848–2852.
42. Binétruy, B. et al. (1991) Ha-Ras augments c-Jun activity and stimulates phosphorylation of its activation domain. Nature, 351, 122–127.
43. Pulverer, B.J. et al. (1991) Phosphorylation of c-jun mediated by MAP kinases. Nature, 353, 670–674.
44. Dérijard, B. et al. (1994) JNK1: a protein kinase stimulated by UV light and Ha-Ras that binds and phosphorylates the c-Jun activation domain. Cell, 76, 1025–1037.

45. Meric-Bernstam, F. et al. (2009) Targeting the mTOR signaling network for cancer therapy. J. Clin. Oncol., 27, 2278–2287.
46. Jhawer, M. et al. (2008) PIK3CA mutation/PTEN expression status predicts response of colon cancer cells to the epidermal growth factor receptor inhibitor cetuximab. Cancer Res., 68, 1953–1961.
47. Weickhardt, A.J. et al. (2010) Strategies for overcoming inherent and acquired resistance to EGFR inhibitors by targeting downstream effectors in the RAS/PI3K pathway. Curr. Cancer Drug Targets, 10, 824–833.
48. Wymann, M.P. et al. (1996) Wortmannin inactivates phosphoinositide 3-kinase by covalent modification of Lys-802, a residue involved in the phosphate transfer reaction. Mol. Cell. Biol., 16, 1722–1733.
49. Vlahos, C.J. et al. (1994) A specific inhibitor of phosphatidylinositol 3-kinase, 2-(4-morpholinyl)-8-phenyl-4H-1-benzopyran-4-one (LY294002). J. Biol. Chem., 269, 5241–5248.
50. Feldman, M.E. et al. (2009) Active-site inhibitors of mTOR target rapamycin-resistant outputs of mTORC1 and mTORC2. PLoS Biol., 7, e38.